Available online at www.eccomasproceedia.org
Eccomas Proceedia COMPDYN (2021) 935-954

ECCOMAS
Proceedia

COMPDYN 2021
8th ECCOMAS Thematic Conference on
Computational Methods in Structural Dynamics and Earthquake Engineering
M. Papadrakakis, M. Fragiadakis (eds.)
Streamed from Athens, Greece, 28 - 30 June 2021

GENERATION OF OUT-OF-PLANE FRAGILITY FUNCTIONS FOR IN-PLANE DAMAGED UNREINFORCED MASONRY INFILLS

Bharat Pradhan[1], Liborio Cavaleri[1], Vasilis Sarhosis[2], Marco Filippo Ferrotto[1*]

[1] University of Palermo
Viale delle Scienze, Palermo
{bharat.pradhan, liborio.cavaleri, marcofilippo.ferrotto}@unipa.it

[2] University of Leeds
LS2 9JT, Leeds, United Kingdom
V.Sarhosis@leeds.ac.uk

Abstract

Fragility assessment of unreinforced masonry (URM) infill walls under seismic loads is a current research topic for large scale risk analysis of reinforced concrete frame structures. In this paper, Out-of-Plane (OoP) fragility functions are developed by probabilistic approach based on Monte Carlo simulations employing a numerical macro-element model for the evaluation of the OoP capacity of infills. Uncertainties in the capacity were considered depending on the level of In-Plane (IP) damage and the variability in the geometrical and mechanical properties of the masonry infills. The fragility functions are therefore obtained considering the variability in the capacity instead of the seismic input as for other studies, considering also their sensitivity to the position in low rise buildings.

Keywords: Fragility, Macro-element model, URM infill, Out-of-plane, IP-OOP interaction.

ISSN:2623-3347
Peer-review under responsibility of the organizing committee of COMPDYN 2021.
doi:10.7712/120121.8536.19549

1 INTRODUCTION

Seismic risk mitigation for reinforced concrete (RC) structures requires the use of reliable strategies for the evaluation of the seismic capacity in view of performing large scale analysis [1]. RC structures exhibit often significant structural and non-structural damage when subjected to medium-to-strong ground shakings. Retrofitting strategies as well as energy dissipation and isolation can be considered effective strategies for the improvement of the seismic behavior of load bearing frame elements such as beams or columns [2-12]. However, non-structural damage related to elements such as infill walls is often neglected in the evaluation of the overall structural behavior.

Damages in infills result in huge economic loss due to a significant downtime and repair cost [13]. Particularly, out-of-plane (OoP) failure can be a big threat to human life. Such infill walls resulted to be highly vulnerable to in-plane (IP) and out-of-plane (OoP) actions caused by seismic loads in past and recent earthquakes [14, 15] and it has been confirmed by a number of experimental studies that OoP capacity of the infills reduce as the IP damage increases [16-20].

Fragility functions are important tools to estimate the probability of OoP collapse of infill walls. But very few works have been done in this direction, often limited because of the computational effort in analyzing a huge number of cases due to variations in infills' properties as well as the IP-OoP interaction [21-23]. Some of the available fragility curves were developed by using macro-element models considering the IP-OOP interaction in determining the OoP strength of infill walls [24-31].

Another important aspect is that the most of the available fragility functions were derived considering the variability in the ground motions (uncertainties in the demand) without taking into account uncertainties in the capacity due to the variability of infill mechanical and geometrical properties and, at the same time, the IP-OoP interaction: this is the main aim of this study for the case of low-rise buildings.

The novel contribution of this work is therefore to consider the variability of the capacity of infills by employing a probabilistic approach based on Monte Carlo simulations including the uncertainties in the mechanical and geometrical properties instead of the variability in the seismic input. The macro-element model proposed by Pradhan and Cavaleri [28] has been used for numerical analysis. The probabilistic approach allowed to consider the uncertainty in the infills' strength and geometric features as well as the uncertainty in the IP drift (inter-storey drift ratio) during an earthquake. Fragility curves have been derived for infill walls built with two types of masonry units (hollow and solid) and interested by three different levels of IP damage: low, medium and high corresponding to three ranges of IP-drift. The fragility curves proposed in this study refer to infills positioned at different floors of low-rise RC frame buildings.

2 PROCEDURE PROPOSAL TO DERIVE FRAGILITY CURVES

2.1 Theoretical framework

For the derivation of OoP fragility curves of masonry infill walls, a probabilistic approach employing a specific range of variability for the input parameter has been implemented by using Monte Carlo simulation. The outputs are therefore affected by random assumption over a range of representative input cases.

To reproduce the physical process using a probabilistic approach, first, a cycle of IP demand randomly assigned is applied to an infilled frame with random geometrical and mechanical characteristics, and then the infill is pushed in OoP direction to determine the capacity

and consequently the Peak Ground acceleration (PGA). Monte Carlo methodology includes the following steps:

1) Random generation of variables such as the thickness and strength of masonry, IP displacement demand, etc.;
2) Calculation of OoP capacity by a macro-element model in OpenSees [32];
3) Determination of the equivalent OoP pseudo (spectral) acceleration;
4) Derivation of the PGA associated to the pseudo acceleration;
5) Determination of the probability of exceedance of OoP collapse and obtaining of the fragility for a given case study.

The above procedure was implemented first in Matlab code for the generation of a random input variables' matrix characterized by a certain number of cases; then, the random matrix was linked to OpenSees [32] to perform numerical analyses, getting the matrix of the results corresponding to each case of analysis. The results obtained by OpenSees were the maximum OoP forces and the corresponding displacements. Additionally, the value of forces, corresponding to one-third of the maximum ones, and the associated OoP displacements, were extracted for each analysis to derive OoP stiffness of the infills.

2.2 Range of parameters and base assumptions

Two fragility groups have been defined for URM infill walls: a) infill with solid masonry units (isotropic property), and b) infill with hollow masonry units (orthotropic property). Additionally, the fragility has been sub-grouped according to the level of IP damage as: low, medium and high (0-0.7%, 0.7-1.4% and 1.4-2% respectively) and the aspect ratios of infills (1.0, 1.25, 1.50 and 1.75). Only one damage state has been considered in the OoP direction i.e. the damage state of collapse. The masonry infill collapse in OoP direction is immediately identified by the OoP pseudo acceleration equal to the ratio between the OoP strength and mass. However, as before-mentioned, the Peak ground acceleration (PGA) has been taken as an Engineering Demand Parameter for the fragility assessment.

Infill walls are bounded by square columns of size 300 mm×300 mm and 300 mm×400 mm beams at top and bottom. Columns are provided with 8 @18 mm longitudinal rebars while the beams have 3 @16 mm rebars at top and bottom. The concrete in the frame members is confined by rectangular stirrups (@ 8 mm) kept at a spacing of 75 mm. The effect of confinement, - provided by the steel reinforcement, as suggested in [33, 34], has been taken in to account according to Mander's model [35]. The yield strength of reinforcement steel is taken as 500 MPa.

For the solid masonry, minimum thickness of infill has been kept as 100 mm while the maximum thickness is assumed to be 200 mm and for the hollow masonry, the thickness was varied from 100 mm to 300 mm. For sake of simplicity, for infill walls built with solid masonry units, the mechanical properties of masonry are assumed as isotropic. In case of masonry with hollow masonry units, orthotropic properties are considered. Elastic modulus of masonry material is assumed as 1000 times the value of compressive strength in both isotropic and orthotropic cases. The main characteristics of the random variables are shown in Table 1. An example of distribution of the compressive strength of masonry for orthotropic and isotropic masonry cases is shown in Fig. 1 a-b.

For each case of low, medium and high IP damage and for each different case of aspect ratio of infill wall, 400 different random samples were generated. Inter-storey drift ratio (IDR) imposed on the infill wall is taken as a measure of IP damage. In Fig. 2a, a sample distribution of IDR to consider three different levels of IP damage is shown while in Fig. 2b, the distribution of the masonry thickness for the case of solid and hollow unit masonry is shown.

Variable	Property	Distribution features
Strength of concrete	Uniform distribution	
	Min (MPa)	20
	Max (MPa)	30
IP damage	Uniform distribution	
	Low level (%)	IDR 0 to 0.7
	Medium level (%)	IDR 0.7 to 1.4
	High Level (%)	IDR 1.4 to 2
Thickness of solid masonry	Uniform distribution	
	Min (mm)	100
	Max (mm)	200
Thickness of hollow masonry	Uniform distribution	
	Min (mm)	100
	Max (mm)	300
Strength of solid masonry (Isotropic behavior)	Gaussian distribution	
	Min (MPa)	3.0
	Max (MPa)	7.0
	Mean (μ)	5.0
	Standard deviation (σ)	1.0
Strength of hollow masonry (Orthotropic behavior)	Gaussian distribution	
	Min (MPa)	1
	Max (MPa)	6
	Mean (μ)	3.5
	Standard deviation (σ)	1.0

Table 1: Distribution of the input parameters.

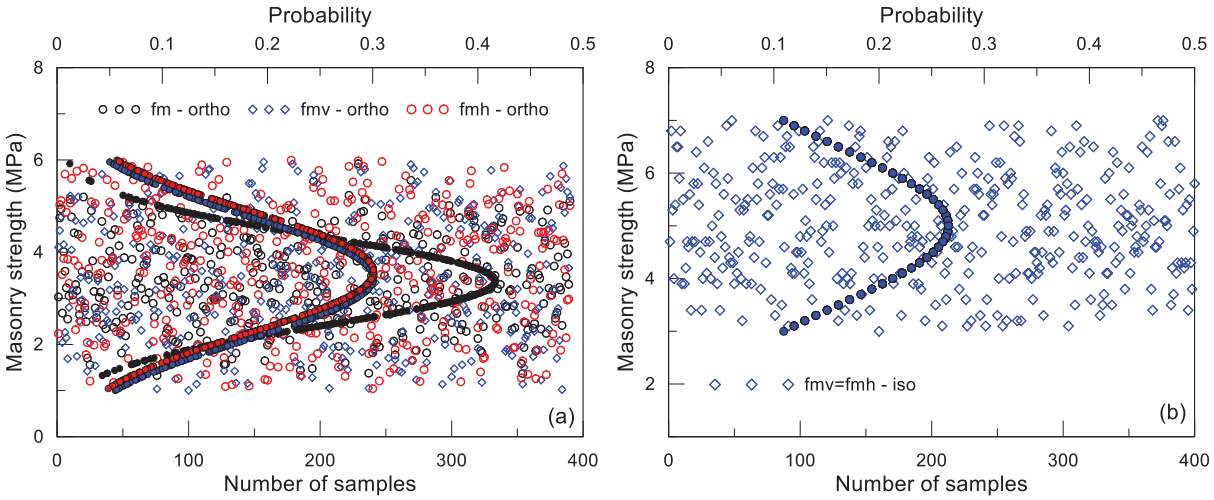

*fmh - ortho, fmv - ortho = Compressive strength of masonry in the horizontal and vertical direction for hollow units

**fm - ortho = Equivalent compressive strength of masonry for hollow units (orthotropic behavior)

***fm - iso = Equivalent compressive strength of masonry for solid units (isotropic behavior)

Figure 1: Distribution of the compressive strength of the masonry: a) orthotropic case (hollow units), b) isotropic case (solid units)

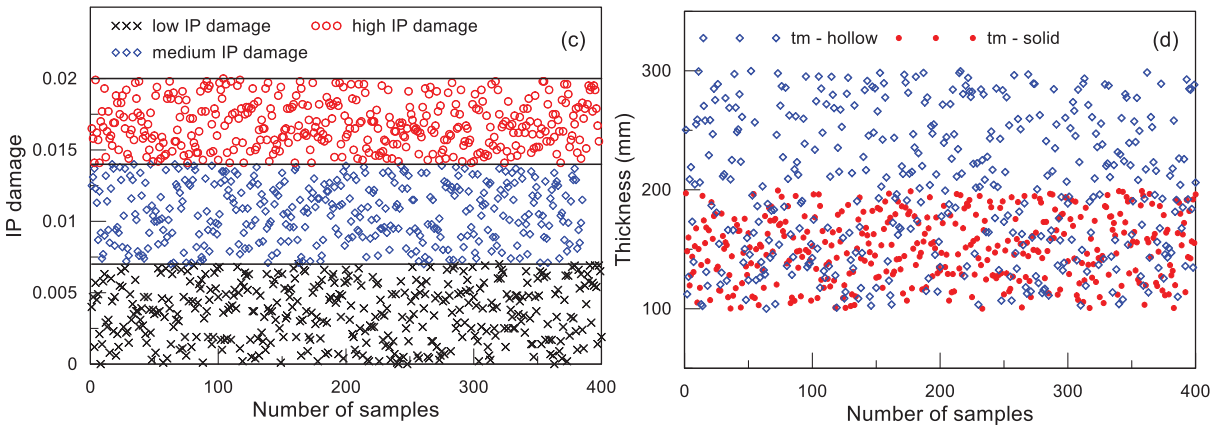

Figure 2: IP damage (a), OOP collapse (b)

2.3 Macro-element modeling of the URM infill walls

The capacity of the panels has been calculated by using macro-element model by Pradhan and Cavaleri [28]. The model consists of four struts (two diagonals, one horizontal and one vertical). The model was validated with results of different experiments [16-18, 29, 36] covering the range of infills' geometrical and mechanical characteristics. Each strut in the model is represented by two fiber-section beam-column elements connected by a node at the mid-span (Fig. 3).

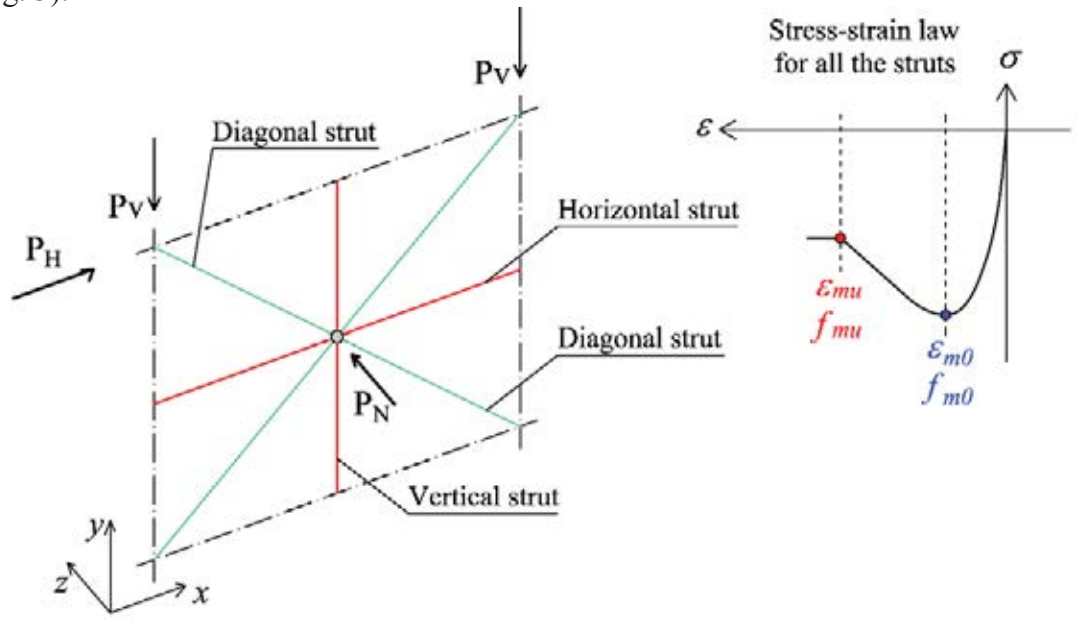

Figure 3: Macro-element model (Pradhan and Cavaleri 2020)

In the model, the width of the diagonal struts w_d is defined as one-third of the diagonal length d while the widths of the horizontal strut w_h and vertical struts w_v are calculated as a function of w_d in the following ways:

$$w_d = d/3 \tag{1}$$

$$d = \sqrt{l'^2 + h'^2} \tag{2}$$

$$w_h = h - w_d / \cos\theta \tag{3}$$

$$w_v = l - w_d / \sin\theta \tag{4}$$

where l and h are the length and height of the infill wall respectively, while l' indicates centre to centre distance between the columns and h' indicates the height of infill plus half the height of top beam and θ is the angle defining the slope of the diagonal struts. In the model, to represent both IP and OoP resistances of the infill wall more accurately, the width and thickness of the diagonal, vertical and horizontal struts were replaced by the surrogated values. For any of the struts with width w and thickness t, surrogated width $\bar{w}$ and surrogate thickness $\bar{t}$ are derived in the following ways:

$$\bar{w} = \frac{f_{mo}}{f_m} \times w \tag{5}$$

$$\bar{t} = \frac{f_m}{f_{mo}} \times t \tag{6}$$

The mechanical properties of the strut fibres in compression are defined by using four stress strain parameters, namely, f_{mo}, f_{mu}, ε_{mo} and ε_{mu} as shown in Fig. 3. These numerical parameters can be calculated based on two different mechanical properties of masonry i.e. the equivalent compressive strength f_m and equivalent elastic modulus E_m, according to the equations provided in Pradhan and Cavaleri [28].

The equivalent properties of masonry, namely f_m and E_m, are derived by taking into account the directional properties following the Eqs. 7-8.

$$f_m = \sqrt{f_{mv} \times f_{mh}} \tag{7}$$

$$E_m = \sqrt{E_{mv} \times E_{mh}} \tag{8}$$

where f_{mv} and f_{mh} represent the masonry's compressive strength in vertical and horizontal directions and E_{mv} and E_{mh} indicate the masonry's elastic modulus respectively in two directions respectively. This provision facilitates the model to consider the orthotropic nature of masonry. The definition of f_m and E_m is purely conventional and this technique relates well with the equivalent strut stress-strain parameters to be used in the model.

For the current study, in case of solid masonry units, the equivalent properties of masonry are derived considering itself as isotropic ($f_{mv} = f_{mh}$ and $E_{mv} = E_{mh}$) and for the case of hollow units as orthotropic. The numerical modelling was performed in OpenSees platform. The concrete and infill materials were modelled by using Concrete02 material, while the steel reinforcement was simulated by using Steel02 material available in OpenSees. The numerical model of any infilled frame was prepared by interfacing Matlab to OpenSees, the former allowed the generation of each set of random parameters. To consider the effect of IP damage in the OoP capacity, IP load was applied to achieve randomly generated IDR demands before the application of OoP load. IP displacement demand was imposed at the top of the infilled frame while OoP load was applied to the centre of the equivalent struts. The OoP capacity of infill walls considering the effect of IP-OoP interaction was thus estimated for all cases investigated.

2.4 Evaluation of PGA from the response spectrum

For a given case, in evaluating the approximate capacity in terms of pseudo (spectral) acceleration, the OoP strength is divided by the mass of the infill wall. In calculating the mass of the infill, density of solid masonry is assumed to be 1900 kg/m^3 in average while for hollow masonry it is assumed as 900 kg/m^3. Each pseudo (spectral) acceleration can be associated to a PGA by the demand spectra.

Demand spectra for non-structural elements like infills depend upon their position along the height of a building, the fundamental period of the infill and the fundamental period of the building [37, 38]. According to the Italian Building Code 2018 [37], the expression of the demand spectrum $S_a\left(T_a, T_1, Z/H\right)$ is given as:

$$S_a = \begin{cases} PGA\left(1+\dfrac{Z}{H}\right)\left[\dfrac{a_p}{1+\left(a_p-1\right)\left(1-\dfrac{T_a}{aT_1}\right)^2}\right] \geq PGA \;\; for \qquad T_a \leq aT_1 \\ PGA\left(1+\dfrac{Z}{H}\right)a_p \qquad\qquad\qquad\qquad for \qquad aT_1 \leq T_a < bT_1 \\ PGA\left(1+\dfrac{Z}{H}\right)\left[\dfrac{a_p}{1+\left(a_p-1\right)\left(1-\dfrac{T_a}{bT_1}\right)^2}\right] \geq PGA \;\; for \qquad T_a \geq bT_1 \end{cases} \tag{9}$$

In the above expression, T_a is the fundamental vibration period of the infill wall, T_1 is the fundamental vibration period of the building, H is the height of the building, and Z is the level at which the infill is located. In Eq. 9, PGA is expressed in g (gravity acceleration). In the present work, the fundamental period of the building is evaluated by means of a simplified equation as follows:

$$T_1 = c \cdot H^{3/4} \tag{10}$$

c being a coefficient depending on the type on the material (0.075 for RC structures). In Eq. 9, the parameters a, b and a_p define the interaction between the infill and the structure depending on the fundamental period T_1 according to Table 2 [39].

	a	b	a_p
T_1<0.5 s	0.8	1.4	5.0
0.5 s < T_1 <1.0 s	0.3	1.2	4.0
T_1>0.5 s	0.3	1.0	2.5

Table 2: Parameters for the response spectrum interaction.

Once the period of the panel T_a and the fundamental period of the structure T_1 are obtained, by imposing the equivalence between the spectral acceleration $S_a(T_a, T_1, Z/H)$ and the pseu-

do-acceleration obtained numerically (that is the infill OoP capacity), it is possible to use Eq. (9) to derive the PGA associated to the infill OoP capacity.

2.5 Evaluation of the fundamental period of the panel

Two different approaches were made in view of calculating the fundamental period of the panel in the OOP direction:

1. By analytical approach proposed by the Italian Building Code 2018 suggestions [37]
2. From the numerical model based on the results of the analyses in terms of stiffness.

Regarding the analytical approach, the fundamental period Ta of the masonry infill in the out-of-plane direction is calculated by the expression given in Eq. (11), where m_w is the mass of the infill per unit height h, E_w is the vertical modulus of elasticity of masonry and I_w is the moment of inertia of the infill horizontal cross section with respect the line obtained as intersection of the middle plane of the infill and the horizontal cross section. Eq. (11) is:

$$T_a = \frac{2h^2}{\pi}\sqrt{\frac{m_w}{K_{red}\cdot E_{wv}\cdot I_{wy}}} \tag{11}$$

It is to be noted that, in evaluating the period of the panel, the reduction in the flexural stiffness due to the IP damage has been considered to obtain a more realistic prediction. To do so, the coefficient K_{red} for the OOP stiffness reduction proposed by Cavaleri et al. [40] was used, that is:

$$K_{red} = [\min(1; 0.17 IDR^{-0.67})] \tag{12}$$

being IDR the inter-storey drift in percentage experienced/assigned by/to the panel in IP direction. The above equation was validated by the authors against a range of experimental and numerical cases.

The second approach is based on the results provided by the numerical analysis depending on the effective stiffness evaluated at one-third of the OoP maximum force and the corresponding displacement. In detail, the numerical period is calculated by using the well-known formula for one degree of freedom system (the equivalent one dof system is that described by the OoP displacement in the center of an infill and the corresponding restoring force) as follows:

$$T_a^* = 2\pi\sqrt{\frac{M^*}{K_{num}}}, \qquad K_{num} = \frac{F_{\max,OOP/3}}{\delta(F_{\max,OOP/3})} \tag{13}$$

In calculating the vibration period, the participating mass M^* corresponding to the first OoP mode of vibration of the infill has been taken as 50% of the total mass of the infill wall. As regard to this choice, different values have been adopted in the literature [21, 22, 23, 29, 31]. The affinity of currently used model with the study of Di Trapani et al [23] oriented such choice of assuming 50% first mode mass in this study.

2.6 Determination of the probability of exceedance of OOP collapse, and obtaining of the fragility for a given case study

Fragility curves are cumulative distribution functions that represent the probability of exceedance of a certain damage state (DS) for a given type of building/structural element over a range of an intensity measure IM (in the context of the present work, the Peak Ground Acceleration "PGA"). A log-normal distribution function can be and is here assumed for the fragility associated to the collapse state according to the following expression:

$$P[DS / IM] = \phi\left(\frac{\ln(IM) - \ln(\overline{IM})}{\beta}\right) \tag{14}$$

where ϕ is the standard normal cumulative distribution function, $\overline{IM}$ refers to a median value and β is the log-standard deviation that accounts for the uncertainties in the capacity of the building/structural element fragilities for the collapse damage state.

In the present study, the uncertainties were assigned for i) the strength of concrete of the reinforced concrete frame surrounding an infill, ii) level of IP damage, iii) thickness of infill, and iv) compressive strength of masonry, employing different distributions of variables. It allowed the evaluation of the median and the log-standard deviation in the results.

3 RESULTS

The fragility curves were obtained in this work assuming low-rise reinforced concrete buildings i.e. 3-storey moment resisting RC frame structure with an inter-storey height of 3 m (total height of the building is 9 m) for which the fundamental period resulted 0.39 sec (Eq. 10). In this context, the fragility was evaluated considering also the influence of the position of the panel with respect to the floors of the structure, evaluating the PGA at collapse state for infill walls placed at the ground storey (first floor) and at the top storey (third floor) of the reference structure.

In the following description of the results, the analyses were labelled depending on the type of masonry (i.e. iso and ortho for solid and hollow masonry respectively), the level of IP damage (i.e. ld, md, hd for low, medium, and high IP damage respectively), the aspect ratio in terms of length-to-height (1.0, 1.25, 1.5, 1.75) and the positioning of the panel with respect to the structure (I and III for the first and the third floor respectively). As an example, the fragility curve iso_ld_1.0_I indicates the fragility for an infilled wall made with solid masonry units, with low IP damage for a panel with aspect ratio 1.0, placed at the first floor, while, the fragility curve ortho_hd_1.5_III indicates the fragility for an infilled wall made with hollow masonry units, with high IP damage for a panel with aspect ratio 1.5, placed at the third floor.. In addition, I or I* and III or III* it is used respectively to give distinction between results calculated by using the period calculated by Eq. (11) (analytical evaluation) or Eq. (13) (by numerical results).

3.1 Influence of the fundamental period in the evaluation of the PGA

The PGAs obtained by using the two different approaches before mentioned for the evaluation of the vibration period of infills in the OoP direction were compared highlighting the sensitivity to the interaction with the response spectrum. In this comparison, the infills placed at the third floor of the low rise reference structure were considered.

First, it has to be noticed that, as expected, the OoP pseudo acceleration as well as the PGA decrease with the increasing level of IP damage and the increasing of the aspect ratio. For a given level of IP damage, infill panels with aspect ratio 1.0 provided higher OoP capacity than panels with aspect ratio 1.25, 1.5 or 1.75. At the same time, for a given value of aspect ratio, infill panels experiencing low levels of IP damage (0.0-0.7%) showed higher capacity compared to that obtained by increasing the level of IP damage (medium and high – drift in the ranges 0.7-1.4% and 1.4-2.0% respectively).

Another consideration has to be done regarding the different responses obtained depending on the type of masonry walls. Overall, it was noticed that hollow masonry showed PGA values higher than solid masonry. This is due to the higher thickness coupled with a low mass of the panels that provided higher pseudo-accelerations and lower vibration periods. Table 3

shows the results for each case of analysis in terms of median values of the PGA and mean values for the vibration period for the two approaches. It is reminded that T_a and T_a^* refer to vibration period calculated by Eq. (11) and Eq. (13) respectively.

At the same time, the vibration period of the panels is affected by the IP damage and aspect ratio. The increasing of the vibration period leads to a different positioning in the response spectrum. It was noticed that with the increasing of the level of IP damage and the increasing of the aspect ratio, the vibration period of the panel increases too and in some cases, it changes from the first branch of the response spectrum ($T<aT_1$) to the second ($aT_1<T<bT_1$). This requires to use a different equation in evaluating the PGA as shown in Eq. (9). This was observed in most of the analysis cases. Having said this, by using Eq. (11), the period of vibration is not much affected by the aspect ratio but only by the level of IP damage. Conversely, by using Eq. (13), the vibration period is significantly influenced both by aspect ratio and IP damage level because the numerical model takes into account the change in stiffness directly. This causes high scatter between T_a and T_a^* that can make the former up to two times the latter. These variations are clearly highlighted in Fig. 4 and Fig. 5 for hollow and solid masonry units respectively. For the above-described reasons, in the subsequent results regarding the evaluation of the fragility curves, it was assumed to evaluate the PGA by using the vibration period calculated from the numerical data to obtain more reliable results.

	Solid masonry – iso (isotropic)											
	low IP damage				medium IP damage				high IP damage			
	Analytical		Numerical		Analytical		Numerical		Analytical		Numerical	
Solid masonry – iso (isotropic)												
Aspect ratio	PGA (g)	Ta (sec)	PGA (g)	Ta* (sec)	PGA (g)	Ta (sec)	PGA (g)	Ta* (sec)	PGA (g)	Ta (sec)	PGA (g)	Ta* (sec)
1	2.32	0.11	2.70	0.06	1.11	0.16	1.68	0.09	0.67	0.19	0.92	0.12
1.25	1.78	0.11	2.29	0.08	0.96	0.15	1.25	0.11	0.48	0.19	0.59	0.13
1.5	1.59	0.10	1.57	0.09	0.69	0.16	0.67	0.13	0.43	0.19	0.45	0.15
1.75	1.25	0.10	1.11	0.10	0.51	0.16	0.46	0.15	0.32	0.19	0.32	0.19
Hollow masonry - ortho (orthotropic)												
1	3.96	0.08	4.78	0.04	1.96	0.11	2.49	0.07	1.22	0.13	1.56	0.09
1.25	3.59	0.07	3.98	0.05	1.50	0.11	1.79	0.08	1.03	0.12	1.14	0.10
1.5	2.64	0.07	2.79	0.06	1.22	0.11	1.29	0.10	0.80	0.13	0.81	0.13
1.75	2.37	0.07	2.30	0.08	1.00	0.11	1.03	0.12	0.63	0.13	0.55	0.15

Table 3: Results of the Monte Carlo simulations for infill walls placed at the third floor of the reference structure.

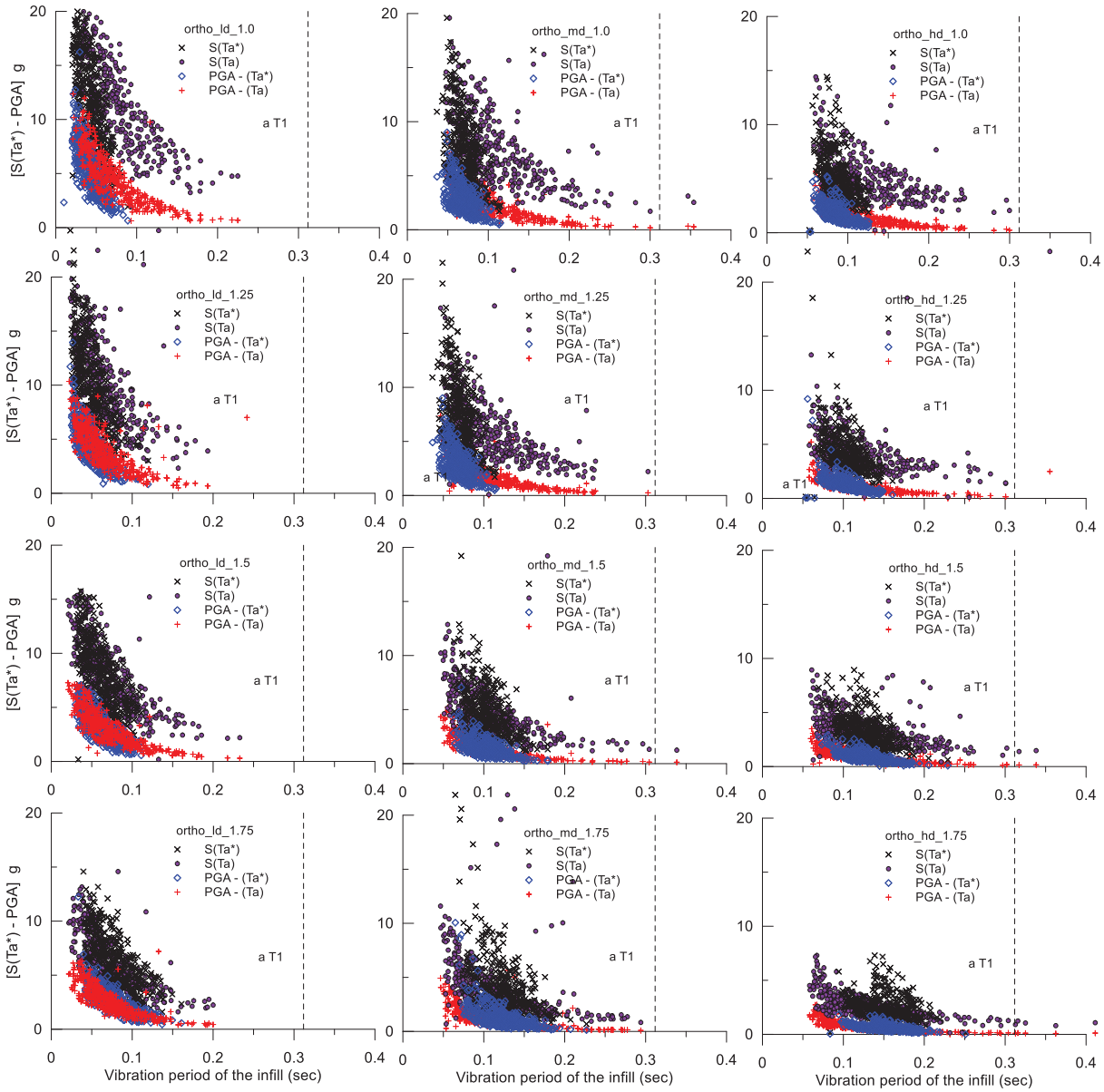

Figure 4: Results of the Monte Carlo simulations: pseudo-acceleration and PGA depending on the vibration period of the infilled walls for the case of orthotropic masonry

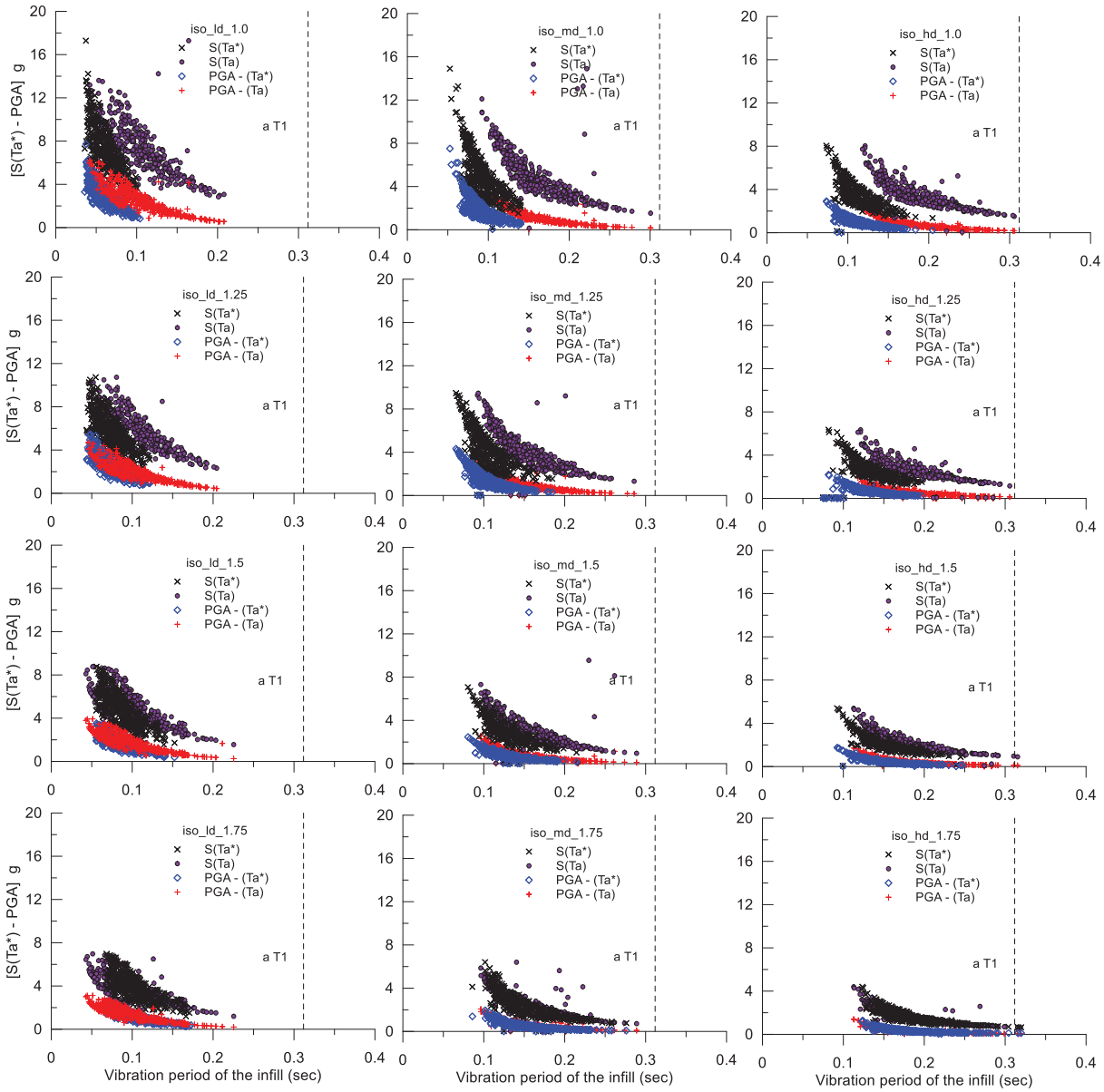

Figure 5: Results of the Monte Carlo simulations: pseudo-acceleration and PGA depending on the vibration period of the infilled walls for the case of isotropic masonry

3.2 OoP fragility curves

The OoP fragility curves obtained by means of the proposed procedure are shown focusing on the influence of the different assumptions during the investigation, which are:

- aspect ratio;
- level of IP damage;
- positioning of the infill panel with respect to the structure;
- type of masonry (solid and hollow units).

The results in terms of fragility curves obtained for solid and hollow units are shown for panels placed at both the first floor and the third floor, considering all the three levels of IP damage (low, medium, high), depending on the aspect ratio of the infill walls. In detail, Figs. 6-7 show the comparisons for given aspect ratio, while Figs. 8-9 show the comparisons for

given range of IP damage. The median and standard deviation values obtained for each case of analysis are shown in Table 4.

The fragility for the panels placed at the top of the reference structure (third floor) resulted to be higher compared to that at the base (first floor) for the same level of IP damage. At the same time, the fragility appeared higher when the level of IP damage and the aspect ratio increased. Overall, what above described was observed for both types of infills made with hollow and solid masonry units. In detail, for aspect ratio 1.0, the PGA (median) values at the first and the third floor resulted of 4.24 g and 2.70 g for the infills with solid units, while for the case of hollow masonry units, the PGA resulted in 7.52 g and 4.78 g respectively. By increasing the aspect ratio from 1.0 to 1.75 and by increasing the level of IP damage from low to high, it was observed that the PGA values dropped to 0.40 g and 0.32 g for the solid masonry units and 0.86 g and 0.55 g for the hollow units. This resulted to be very important in view of showing the high variability in the results depending upon different assumptions.

Based on the results, it can be stated that, in the absence of previous IP damage, the infilled frames provide a high strength and high PGA in the out-of-plane direction. Consequently, lower vulnerability is obtained. On the other hand, in the presence of previous IP damage, regardless of whether it is medium or high, the strength in the OoP direction drops to critical values, providing to the infilled frames very high vulnerability for low values of PGA especially at higher floors and for high values of aspect ratio. To clarify better what above described, the fragility curves for infilled frames with different aspect ratio at high level of IP damage, placed at the top of the reference 3-storey RC structure, are shown in Fig. 10for both type of masonry walls (solid and hollow units).

	ld I	ld III		md I	md III		hd I	hd III	
Aspect ratio	median		std dev	median		std dev	median		std dev
PGA iso (g)									
1	4.24	2.70	1.49	2.13	1.68	1.72	1.44	0.92	1.70
1.25	2.90	2.29	1.50	1.59	1.25	2.00	0.92	0.59	2.01
1.5	2.46	1.57	1.53	1.06	0.67	2.15	0.71	0.45	1.81
1.75	1.74	1.11	1.58	0.73	0.46	2.24	0.40	0.32	1.65
PGA ortho (g)									
1	7.52	4.78	1.63	3.92	2.49	1.66	2.45	1.56	1.63
1.25	6.25	3.98	1.64	2.81	1.79	1.73	1.79	1.14	1.77
1.5	4.38	2.79	1.67	2.02	1.29	1.73	1.27	0.81	1.73
1.75	3.48	2.30	1.67	1.31	1.03	1.97	0.86	0.55	1.70

Table 4: Results of the Monte Carlo simulations for infill walls placed at the third floor of the reference structure.

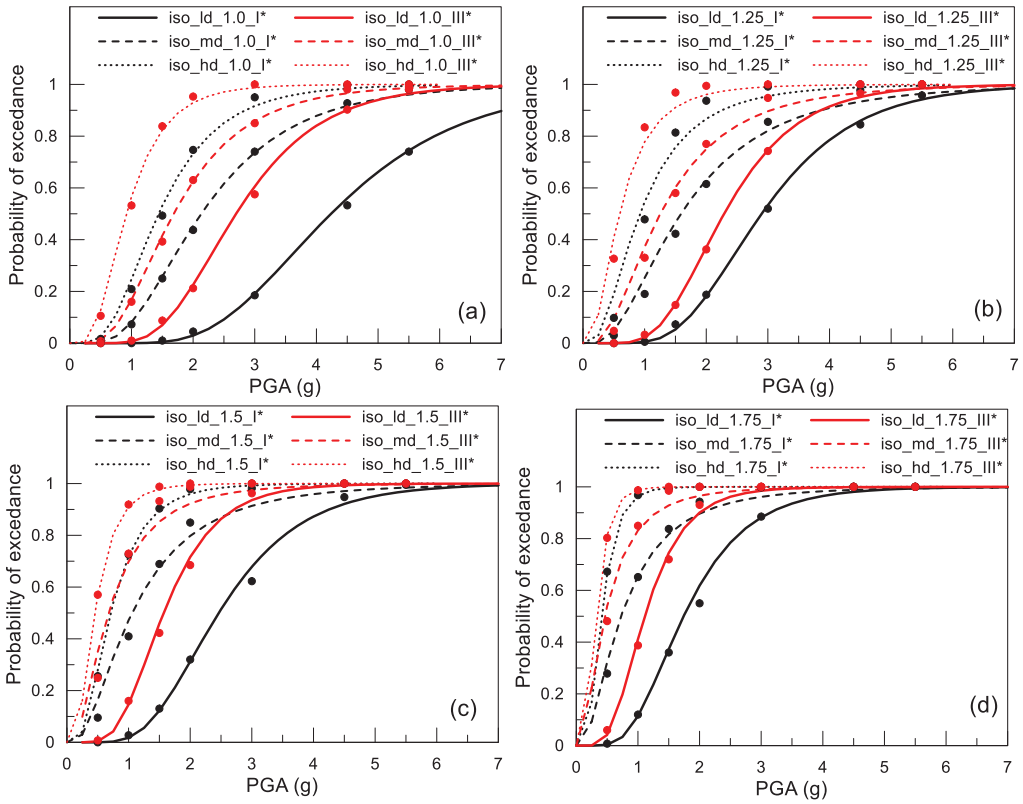

Figure 6: Fragility curves for solid masonry including low, medium and high IP damage for different aspect ratio: a) 1.0, b) 1.25, c) 1.5, d) 1.75.

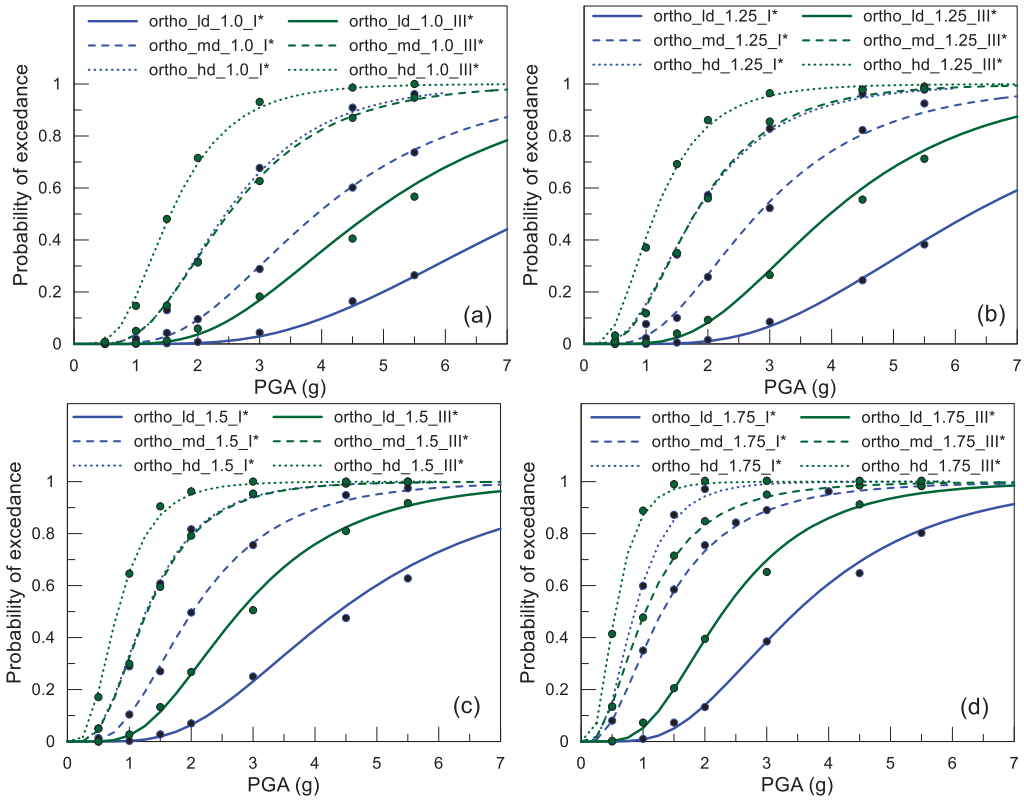

Figure 7: Fragility curves for hollow masonry including low, medium and high IP damage for different aspect ratio: a) 1.0, b) 1.25, c) 1.5, d) 1.75.

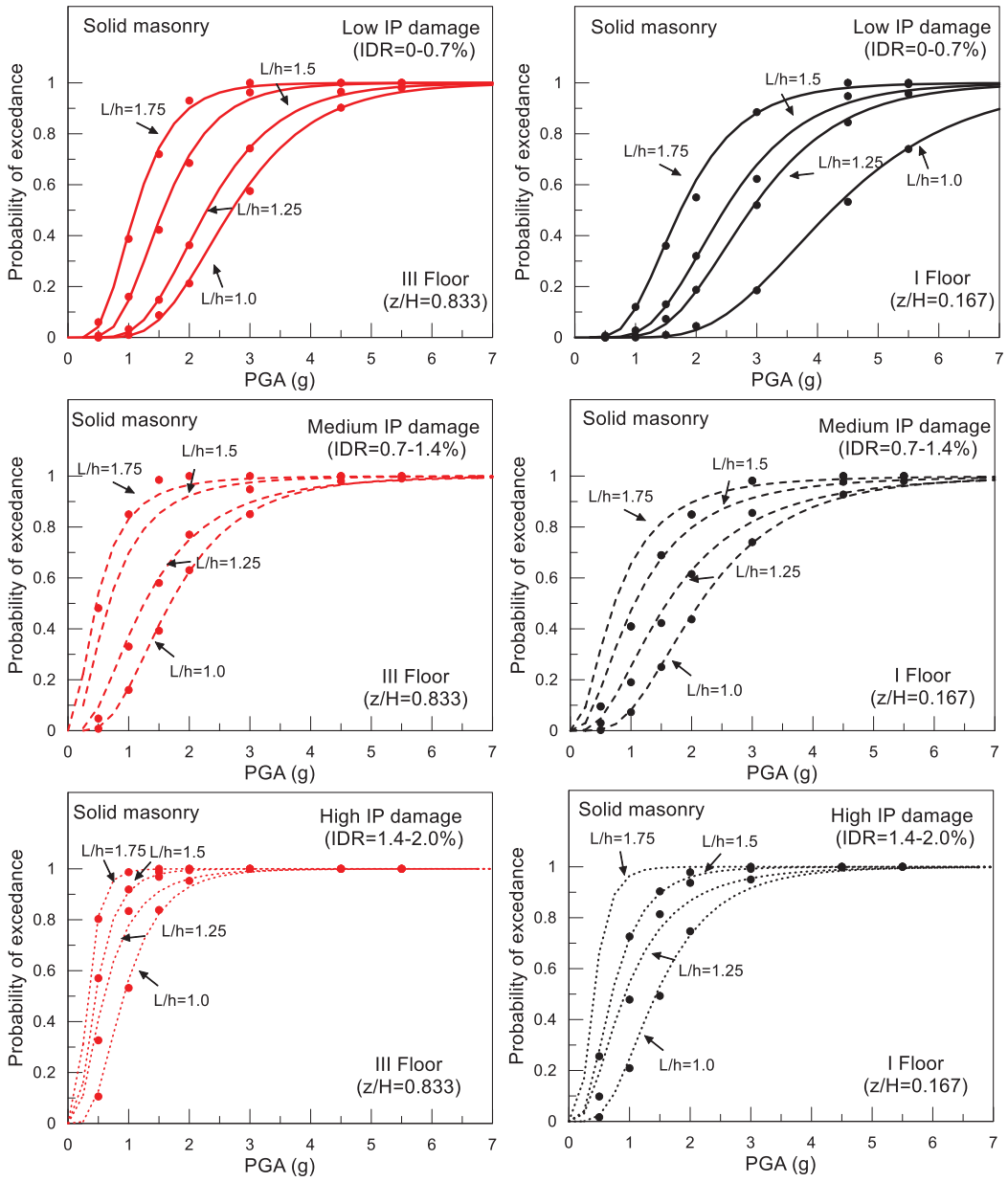

Figure 8: Fragility curves for solid masonry: influence of the aspect ratio for a given level of IP damage.

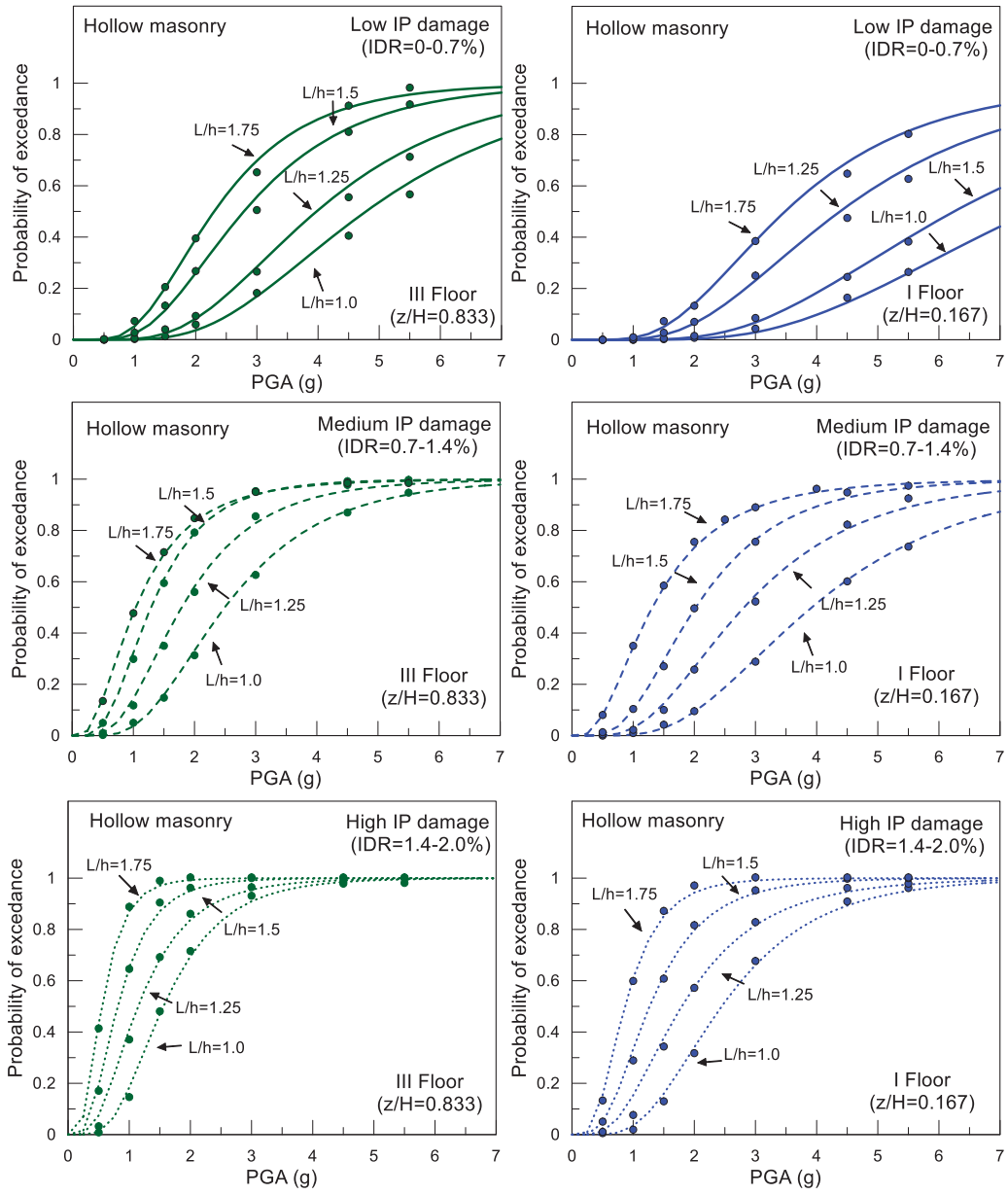

Figure 9: Fragility curves for hollow masonry: influence of the aspect ratio for a given level of IP damage.

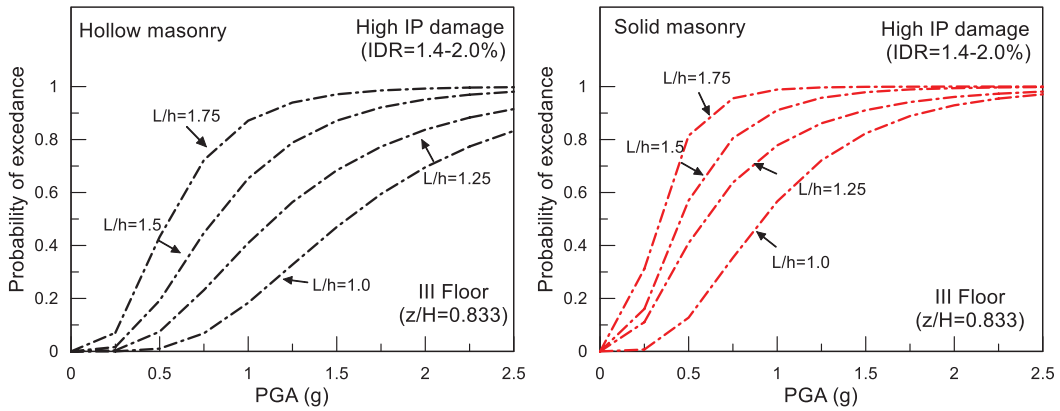

Figure 10: Page layout. Fragility for infilled frames with high IP damage placed at the top of the three-storey reference RC structure.

4 CONCLUSIONS

This paper presented a procedure for the derivation of infill walls out-of-plane fragility functions for low rise RC buildings with respect to the Peak Ground Acceleration (PGA) at collapse. A probabilistic procedure was employed based on Monte Carlo simulations, generating random input variables such as geometrical and mechanical characteristics of the panels and in-plane damage, assuming significant variations. Differently from available studies dealing with infill walls OoP fragility, the novel contribution of the present work was to take into account the uncertainties the capacity instead of in the demand. In evaluating the results, different aspects were investigated such as the influence of the aspect ratio, the influence of the level of IP damage, the influence of the positioning of the infill panel with respect to the structure and the influence of the type of masonry (solid and hollow units).

The results indicated that the OoP fragility of the infill walls increases as the level of IP damage increases as well as for the increasing of the aspect ratio. In the presence of previous IP damage, regardless of whether it is medium or high, the strength in the OOP direction drops to critical values, providing very high fragility for low values of PGA. In addition, for a given level of IP damage and aspect ratio at all floor levels from bottom to the top, the probability of collapse resulted to be higher for panels placed at the top of the structure than those placed at the base of the structure, where the pseudo acceleration of the structure is higher too.

Moreover, for the ranges assumed in this study, high PGA at collapse i.e. lower fragility was observed for infill walls made with hollow masonry units in comparison to infills made with solid masonry units.

REFERENCES

[1] P. Ricci, F. De Luca, G.M. Verderame. 6th April 2009 L'Aquila earthquake, Italy: reinforced concrete building performance. *Bulletin of Earthquake Engineering*, **9**(1), 285–305, 2011.

[2] M.F. Ferrotto, L. Cavaleri, F. Di Trapani, FE modeling of Partially Steel-Jacketed (PSJ) RC columns using CDP model, *Computers and Concrete*, **22**,143-152 2018.

[3] M.F. Ferrotto, O. Fischer, L. Cavaleri. A strategy for the finite element modeling of FRP-confined concrete columns subjected to preload, *Engineering Structures*, **173** (2018), 1054-1067.

[4] M.F. Ferrotto, L. Cavaleri, M. Papia. Compressive response of substandard steel jacketed RC columns strengthened under sustained loads: from the local to the global behavior. *Construction and Building Materials*, **179** (2018), 500-511.

[5] G. Campione, F. Cannella, M.F. Ferrotto. M. Gianquinto. Compressive behavior of FRP externally wrapped R.C. column with buckling effects of longitudinal bars. *Engineering Structures*, **168**, 809–818, 2018.

[6] M.F. Ferrotto, O. Fischer, L. Cavaleri. Analysis-oriented stress–strain model of CRFP-confined circular concrete columns with applied preload. *Matererials and Structures*, 51:44, 2018. https://doi.org/10.1617/s11527-018-1169-0.

[7] G. Campione, L. Cavaleri, F. Di Trapani, M.F. Ferrotto. Frictional effects on structural behavior of no-end-connected steel-jacketed RC columns: Experimental results and new approaches to model numerical and analytical response, *Journal of Structural Engineering ASCE*, **143**,04017070, 2017. DOI: 10.1061/(ASCE)ST.1943-541X.0001796.

[8] M.F. Ferrotto, O. Fischer, R. Niedermeier. Experimental Investigation on the Compressive Behavior of Short Term Preloaded CFRP-Confined Concrete Columns. *Structural Concrete*,1-14, 2017. DOI:10.1002/suco.201700072.

[9] G. Alotta, L. Cavaleri, M. Di Paola, M.F. Ferrotto. Solution for the Design and Increasing of Efficiency of Viscous Dampers, *The Open Construction and Building Technology Journal*, 10, (Suppl 1: M6) 106-121, 2016.

[10] L. Cavaleri, F. Di Trapani, M.F. Ferrotto. Experimental determination of viscous dampers parameters in low velocity ranges. *Ingegneria Sismica*, **34**(2), 64-74, 2017.

[11] M.F. Ferrotto, P.G. Asteris, L. Cavaleri. Strategies of Identification of a Base-Isolated Hospital Building by Coupled Quasi-Static and Snap-Back Tests, *Journal of Earthquake Engineering*, 2020. DOI: 10.1080/13632469.2020.1824877;

[12] M.F. Ferrotto, L. Cavaleri, F. Di Trapani, P. Castaldo. Full scale tests of the base-isolation system for an emergency hospital. *In COMPDYN 2019 7th International Conference on Computational Methods in Structural Dynamics and Earthquake Engineering* - vol.1 (pp. 2012-2025), 2019. M. Papadrakakis, M. Fragiadakis (eds.). Crete, Greece, 24–26 June 2019.

[13] C. Del Vecchio, M. Di Ludovico, S. Pampanin, A. Prota, A. Repair Costs of Existing RC Buildings Damaged by the L'Aquila Earthquake and Comparison with FEMA P-58 Predictions. *Earthquake Spectra*, **34**(1), 237–263, 2018.

[14] F. Braga, V. Manfredi, A. Masi, A. Salvatori, M. Vona. Performance of non-structural elements in RC buildings during the L'Aquila, 2009 earthquake." *Bulletin of Earthquake Engineering*, **9**(1), 307–324, 2011.

[15] H. Varum, A. Furtado, H. Rodrigues, L. Dias-Oliveira, N. Vila-Pouca, A. Arêde. "Seismic performance of the infill masonry walls and ambient vibration tests after the Ghorka 2015, Nepal earthquake. *Bulletin of Earthquake Engineering*, **15**(3), 1185–1212, 2017.

[16] R. Angel, D. Abrams, D. Shapiro, J. Uzarski, M. Webster. *Behavior of reinforced concrete frames with masonry infills*. ISSN: 0069-4274, University of Illinois at Urbana-Champaign, Illinois, 1994.

[17] F. Da Porto, G. Guidi, M.D. Benetta, N. Verlato. Combined in-plane/out-of-plane experimental behavior of reinforced and strengthened infill masonry walls. *12th Canadian masonry symposium*, **12**, 2013.

[18] M.T. De Risi, M. Di Domenico, P. Ricci, G.M. Verderame, G. Manfredi. Experimental investigation on the influence of the aspect ratio on the in-plane/out-of-plane interaction for masonry infills in RC frames. *Engineering Structures*, **189**, 523–540, 2019.

[19] S. Hak, P. Morandi, G. Magenes. Out-of-plane experimental response of strong masonry infills. *In: 2nd European conference on earthquake engineering and seismology*, 12, 2014.

[20] P. Ricci, M. Di Domenico, G.M. Verderame. Experimental investigation of the influence of slenderness ratio and of the in-plane/out-of-plane interaction on the out-of-plane strength of URM infill walls. *Construction and Building Materials*, **191**, 507–522, 2018.

[21] M. Di Domenico, P. Ricci, G.M. Verderame. Empirical unreinforced masonry infill macro-model accounting for in-plane/out-of-plane interaction. *In: Proceedings of the 6th International Conference on Computational Methods in Structural Dynamics and Earthquake Engineering* (COMPDYN 2017), Institute of Structural Analysis and Antiseismic Research School of Civil Engineering National Technical University of Athens (NTUA) Greece, Rhodes Island, Greece, 1606–1624, 2017.

[22] G. Gesualdi, L.R.S. Viggiani, D. Cardone, D. Seismic performance of RC frame buildings accounting for the out-of-plane behavior of masonry infills. *Bulletin of Earthquake Engineering*, **18**(11), 5343–5381, 2020.

[23] F. Di Trapani, M. Malavisi, P.B. Shing, L. Cavaleri. Definition of out-of-plane fragility curves for masonry infills subject to combined in-plane and out-of-plane damage. Brick and Block Masonry - From Historical to Sustainable Masonry, J. Kubica, A. Kwiecień, and Ł. Bednarz, eds., CRC Press, 943–951, 2020.

[24] S. Kadysiewski, K.M. Mosalam. Modeling of Unreinforced Masonry Infill Walls Considering In-Plane and Out-of-Plane Interaction. PEER 2008/102, University of California, Berkeley, **144**, 2009.

[25] K.M. Mosalam, S. Günay. Progressive Collapse Analysis of RC Frames with URM Infill Walls Considering In- Plane/Out-of-Plane Interaction. *Earthquake Spectra*, **26**, 2015.

[26] A. Furtado, H. Rodrigues, A. Arêde, H. Varum. Simplified macro-model for infill masonry walls considering the out-of-plane behaviour: Macro-model for Infill Walls Considering the Out-of-plane Behaviour." Earthquake Engineering & Structural Dynamics, 45(4), 507–524, 2016.

[27] F. Di Trapani, P.B. Shing, L. Cavaleri. Macroelement Model for In-Plane and Out-of-Plane Responses of Masonry Infills in Frame Structures. *Journal of Structural Engineering*, **144**(2), 04017198, 2018.

[28] B. Pradhan, L. Cavaleri. IP-OOP interaction in URM infilled frame structures: A new macro-modelling proposal. *Engineering Structures*, **224**, 111211, 2020.

[29] P. Ricci, M. Di Domenico, G.M. Verderame. Empirical-based out-of-plane URM infill wall model accounting for the interaction with in-plane demand. *Earthquake Engineering & Structural Dynamics*, **47**(3), 802–827, 2018.

[30] P. Ricci, M. Di Domenico, G.M. Verderame. Nonlinear dynamic assessment of the out-of-plane response and behaviour factor of unreinforced masonry infills in reinforced concrete buildings. Proceedings of the 7th International Conference on Computational Methods in Structural Dynamics and Earthquake Engineering (COMPDYN 2019), Institute of Structural Analysis and Antiseismic Research School of Civil Engineering National Technical University of Athens (NTUA) Greece, Crete, Greece, 2103–2115, 2019.

[31] P. Ricci, M. Di Domenico, G.M. Verderame. Effects of the In-Plane/Out-of-Plane Interaction in URM Infills on the Seismic Performance of RC Buildings Designed to Eurocodes. *Journal of Earthquake Engineering*, 1–35, 2020.

[32] F. McKenna, G.L. Fenves, M.H. Scott. Open system for earthquake engineering simulation. University of California, Berkeley, CA. 2000.

[33] G. Campione, L. Cavaleri, M.F. Ferrotto, G. Macaluso, M. Papia. Efficiency of Stress-Strain Models of Confined Concrete With and Without Steel Jacketing to Reproduce Experimental Results. *The Open Construction and Building Technology Journal*, **10**, (Suppl 1: M4) 65-86, 2016.

[34] L. Cavaleri, F. Di Trapani, M.F. Ferrotto, L. Davì. Stress-Strain Models for Normal and High Strength Confined Concrete: Test and Comparisons of Literature Models Reliability in Reproducing Experimental Results. *Ingegneria Sismica*, **34**, Special Issue B, 114-137, 2017.

[35] J.B. Mander, M.J.N. Priestley, R. Park. Theoretical Stress ‐ Strain Model for Confined Concrete. *Journal of Structural Engineering*, **114**(8), 1804 ‐ 1826, 1988.

[36] G.M. Calvi, D. Bolognini, D. Seismic response of reinforced concrete frames infilled with weakly reinforced masonry panels. *Journal of Earthquake Engineering,* **5**(2), 153–185, 2001.

[37] NTC 2018. Decreto Ministeriale delle Infrastrutture e dei Trasporti 17 gennaio 2018, Aggiornamento delle «Norme tecniche per le costruzioni»

[38] EN 1998-1. 2004. Eurocode 8: Design of Structures for Earthquake Resistance - Part 1: General Rules, Seismic Actions and Rules for Buildings. European Committee for Standardization, Brussels.

[39] Circolare 21 gennaio 2019, n. 7 C.S.LL.PP. Istruzioni per l'applicazione dell'«Aggiornamento delle "Norme tecniche per le costruzioni"» di cui al decreto ministeriale 17 gennaio 2018

[40] L. Cavaleri, M. Zizzo, P.G. Asteris. Residual out-of-plane capacity of infills damaged by in-plane cyclic loads. *Engineering Structures*, 109957, 2019.